Li *et al. Chem Synth* 2024;4:22
DOI: 10.20517/cs.2023.69

Chemical Synthesis

Research Article

Open Access

Check for updates

Biological metal–organic frameworks for natural gas purification and MTO product separation

Wen Li[1], Dan Wang[1], Yi Wang[2], Zhaohui Shi[1], Junxue Liu[1], Lirong Zhang[1], Dongxu Xue[2], Yunling Liu[1,*]

[1]State Key Laboratory of Inorganic Synthesis and Preparative Chemistry, College of Chemistry, Jilin University, Changchun 130012, Jilin, China.
[2]Key Laboratory of Applied Surface and Colloid Chemistry, Ministry of Education, Xi'an Key Laboratory of Organometallic Material Chemistry, School of Chemistry & Chemical Engineering, Shaanxi Normal University, Xi'an 710062, Shaanxi, China.

[*]**Correspondence to:** Prof. Yunling Liu, State Key Laboratory of Inorganic Synthesis and Preparative Chemistry, College of Chemistry, Jilin University, 2699 Qianjin Street, Changchun 130012, Jilin, China. E-mail: yunling@jlu.edu.cn

How to cite this article: Li W, Wang D, Wang Y, Shi Z, Liu J, Zhang L, Xue D, Liu Y. Biological metal–organic frameworks for natural gas purification and MTO product separation. *Chem Synth* 2024;4:22. https://dx.doi.org/10.20517/cs.2023.69

Received: 26 Dec 2023 **First Decision:** 7 Mar 2024 **Revised:** 11 Mar 2024 **Accepted:** 28 Mar 2024 **Published:** 8 Apr 2024

Academic Editor: Alain Krief **Copy Editor:** Pei-Yun Wang **Production Editor:** Pei-Yun Wang

Abstract

The use of porous solid adsorbents is an effective and excellent approach for the separation and purification of methanol-to-olefins product and methane (CH_4). In this particular study, a series of adenine (AD)-based biological metal–organic frameworks (Bio-MOFs) {Their general formula is **$Cu_2(AD)_2(X)_2$** [X = formic acid, acetic acid (AA), and propionic acid]} were proposed, which exhibited remarkable efficiency in the purification of CH_4 and the separation of C_3H_6 from methanol-to-olefins product, ultimately yielding purified C_2H_4. The experimental findings demonstrate that different terminal ligands induce alterations in the pore microenvironment, consequently leading to variations in adsorption capacities and stability. Specifically, **Cu-AD-AA** exhibits the highest adsorption capacity and selectivity among the three MOFs, as confirmed by static adsorption isotherm testing and theoretical evaluation using ideal adsorbed solution theory (IAST) simulation. At 298 K and 1 bar, **Cu-AD-AA** exhibits 786 and 10.9 selectivity for C_3H_8/CH_4 and C_3H_6/C_2H_4, respectively, surpassing the majority of MOFs materials. Furthermore, breakthrough experiments conducted in ambient conditions reveal that **Cu-AD-AA** possesses commendable separation capabilities, enabling one-step purification of C_2H_4 at varying proportions (C_2H_4/C_3H_6 = 50:50, 50:20, and 90:10), along with satisfactory recycling performance. Importantly, the synthesis of **Cu-AD-AA** utilizes simple and easily obtainable raw materials, thereby offering advantages such as cost-effectiveness, low toxicity, and facile synthesis that enhance its potential for industrial applications.

Keywords: Bio-MOFs, MTO product separation, natural gas purification, porous solid adsorbents

INTRODUCTION

In recent years, light hydrocarbons as important chemical raw materials and fuels have gained significant application in various fields[1,2]. Natural gas is widely recognized as a clean energy that can be extensively applied in power generation, domestic fuel, and even in the automotive industry[3-5]. Pyrolysis gas, which is a major source of natural gas, primarily consists of methane (CH_4) and light hydrocarbons (C_2-C_3) such as acetylene (C_2H_2), ethylene (C_2H_4), ethane (C_2H_6), and propane (C_3H_8)[6,7]. However, the presence of these light hydrocarbon impurities not only decreases the conversion rate of CH_4 but also affects the stability of cyclic processes during storage and the safe transportation through pipelines. Therefore, it is necessary to remove these impurities to ensure the purity of the natural gas before it can be liquefied and transported[8]. Interestingly, these C_2 and C_3 light hydrocarbons also serve as essential raw materials in the petrochemical industry. Effective separation of these light hydrocarbons from pyrolysis gas not only enhances the purity of CH_4 but also enables efficient utilization of C_2-C_3 molecules.

In addition to CH_4 purification, the industrialization of the methanol-to-olefins (MTO) reaction has witnessed significant advancements in recent years[9,10]. MTO reaction is a significant and advanced method for producing C_2H_4 from coal and natural gas, with the product consisting of approximately 21 wt% C_3H_6 and 51 wt% C_2H_4[11,12]. Therefore, the separation of C_3H_6 and C_2H_4 in MTO product is crucial for downstream applications[13,14]. However, the separation of C_3H_6 and C_2H_4 poses a complex and challenging task due to their relatively low boiling points (225.4 K for C_3H_6 and 169.4 K for C_2H_4) and similar kinetic diameters (4.6 Å for C_3H_6 and 4.2 Å for C_2H_4)[15-17]. Due to the relatively low boiling point of these light hydrocarbons, conventional methods for separating light hydrocarbons often rely on high pressure and low temperature distillation processes. Nevertheless, this approach suffers from several drawbacks including high energy consumption, large footprint, and complex operation[18]. To address these issues, combining physical adsorbents with pressure swing adsorption (PSA) technology has emerged as a promising alternative[19]. This method, based on the principle of physical adsorption, can be conducted at ambient temperature and pressure, not only offering a simple operational procedure but also ensuring low energy consumption. Among various physical adsorbents, metal–organic frameworks (MOFs) materials have gained significant attention in materials science due to their excellent properties[20-22].

MOFs are crystalline structures formed through coordination bonds between metal ions or clusters and organic ligands[23-25], which exhibit higher specific surface area, porosity, and adjustable structure compared to traditional materials such as porous silicon, activated carbon, and zeolite[26-28]. As a result, it offers a broader range of potential applications; for example, it has fantastic uses in the fields of gas adsorption and separation, energy conversion, drug delivery, water vapor capture, catalysis, and sensing[29-33]. In industrial settings, MOFs materials can be designed to purify natural gas and separate MTO product based on slight physical differences between these light hydrocarbons[34]. For example, C_3H_8 and C_2H_6 molecules have slightly larger sizes and polarizabilities than CH_4. By designing pore size close to C_3H_8 and C_2H_6 molecules and enhancing interaction between the framework and gas molecules, efficient natural gas purification can be achieved[35]. Similarly, for C_3H_6 and C_2H_4, pores can be designed based on their difference in polarizability, and the introduction of specific organic functional groups can increase the van der Waals interaction between the host material and guest molecules, thereby facilitating the efficient separation of C_3H_6/C_2H_4 mixtures[36]. In addition, MOFs materials, which operate on the principles of physical adsorption, possess low adsorption enthalpy, exceptional thermal stability, and regenerability, enabling efficient adsorption and desorption at moderate temperatures. This characteristic can significantly save energy consumption[37].

Thanks to the progress of reticular chemistry, MOFs materials have enabled precise regulation of pore environments to selectively adsorb specific gas molecules[38]. Generally, two strategies are employed for regulating pores in MOFs. One involves substituting metal ions to achieve sub-angstrom precision regulation[39], while the other adjusts ligands to accurately regulate the structure by altering the length and introducing functional groups[40,41]. However, the first approach is limited by different coordination modes of metal ions and restricted choices of metals, making it difficult for widespread use. In contrast, the second technique, which utilizes organic ligands, is more commonly adopted due to the wide range of options available. In the pursuit of industrial-grade production, factors such as environmental friendliness and cost-effectiveness must be considered. Traditional MOFs heavily rely on ligands produced through organic synthesis[42]. Many of these ligands, particularly those with special functional groups (such as -NH_2, -CH_3, -CH_2CH_3 and -CF_3), require customization, leading to significant costs. Moreover, most of these ligands are toxic and unsuitable for large-scale production. In contrast, Bio-MOFs composed of biomolecules and metal ions have gained attention among various MOFs materials due to their low cost, low toxicity, good reproducibility, and adherence to the principles of green chemistry[43,44]. Inexpensive biomolecules, such as amino acids, proteins, peptides, and porphyrins, can serve as ligands for synthesizing Bio-MOFs[45,46]. However, the study of Bio-MOFs for light hydrocarbon separation remains relatively limited compared to their use in carbon dioxide capture[47,48].

Based on the aforementioned considerations, we have developed a solvothermal synthesis method for three Bio-MOFs with the traditional **lvt** topology. The rigid ligand adenine (AD), abundant in nitrogen atoms and amino groups, is an excellent choice for constructing stable MOFs with active sites. While **Cu-AD-AA** and **Cu-AD-PA** structures were previously reported using diffusion methods, in this study, we successfully synthesized them through solvothermal techniques[49], which are simpler and more scalable for large-scale production, resulting in defect-free crystals suitable for gas separation applications. **Cu-AD-FA** was reported for the first time, and its structure was analyzed by single-crystal X-ray diffraction experiments. Structural analysis reveals that different terminal carboxylic acid ligands significantly influence the pore environment (channel size, pore volume, active site) of materials. It is noteworthy that previous researchers have conducted some gas adsorption and separation studies for **Cu-AD-AA** and **Cu-AD-PA** materials. For example, in 2012, Pérez-Yáñez *et al.* explored the CO_2/H_2 and CO/H_2 separation properties of these two materials[50]. Similarly, in 2020, Li *et al.* investigated the separation performance of **Cu-AD-PA** specifically for C_2H_2/CO_2[51]. However, a comprehensive investigation into the separation ability of light hydrocarbons, especially for C_2H_4/C_3H_6 separation, has not been done so far. Therefore, the light hydrocarbon adsorption separation of these materials was systematically studied in this work. Among them, **Cu-AD-AA** has exhibited excellent adsorption and separation capacity, demonstrating great potential in natural gas purification and MTO product separation.

EXPERIMENTAL

Materials and methods

The chemicals used in this investigation were acquired from commercial sources and were not subjected to further purification. Scanning electron microscope (SEM) images were captured using a JEOL JSM-7800F microscope. Dynamic light scattering measurements were conducted at 25 °C on a Malvern Zetasizer Nano-ZS90 instrument (detection range: 3-3,000 nm). Powder X-ray diffraction (PXRD) data were collected using a Rigaku D/max-2550 diffractometer with Cu-Kα radiation (λ = 1.5418 Å). Thermogravimetric analysis (TGA) data were obtained using a TGA Q500 thermogravimetric analyzer under air conditions at a heating rate of 10 °C min^{-1}. Surface area was measured using N_2 adsorption isotherms at 77 K with a Micromeritics ASAP 2420 instrument. CH_4, C_2H_2, C_2H_4, C_2H_6, C_3H_6 and C_3H_8 adsorption isotherms were determined using a Micromeritics ASAP 2020 instrument. The breakthrough experiments were conducted in a homemade HPMC41 gas separation test system (Nanjing Hope Analytical Equipment Co., Ltd).

Synthesis of Cu-AD-FA

A mixture of $Cu(NO_3)_2 \cdot 3H_2O$ (12 mg, 0.05 mmol), AD (16 mg, 0.12 mmol), N,N-dimethylformamide (DMF, 2.0 mL) and FA (0.3 mL) was sealed in a 20 mL vial and heated at 65 °C for 24 h. The green octahedron crystals were gathered and washed with EtOH and then dried in air [20 mg, yield 64%, based on $Cu(NO_3)_2 \cdot 3H_2$].

Synthesis of Cu-AD-AA

A mixture of $Cu(NO_3)_2 \cdot 3H_2O$ (2.4 g, 0.010 mol), AD (3.2 g, 0.024 mol), N,N-dimethylacetamide (DMA, 100 mL), H_2O (30 mL) and AA (70 mL) was sealed in a 250 mL vial and heated at 65 °C for 24 h. The green powders were gathered and washed with EtOH and then dried in air [3.12 g, yield 61%, based on $Cu(NO_3)_2 \cdot 3H_2O$]. The microcrystals of **Cu-AD-AA** exhibit a regular octahedral shape which was examined by SEM tests [Supplementary Figure 1A]. These microcrystals reveal an average diameter of 615 nm, as determined by dynamic light scattering tests [Supplementary Figure 1B].

Synthesis of Cu-AD-PA

A mixture of $Cu(NO_3)_2 \cdot 3H_2O$ (2.4 g, 0.010 mol), AD (3.2 g, 0.024 mol), N-Methyl-2-pyrrolidone (NMP, 100 mL), H_2O (30 mL) and PA (60 mL) was sealed in a 250 mL vial and heated at 65 °C for 24 h. The green powders were gathered and washed with EtOH and then dried in air [3.07 g, yield 57%, based on $Cu(NO_3)_2 \cdot 3H_2O$]. The microcrystals of **Cu-AD-PA** exhibit a regular octahedral shape as examined using SEM tests [Supplementary Figure 1C]. These microcrystals reveal an average diameter of 615 nm as determined by dynamic light scattering tests [Supplementary Figure 1D]. The container photographs for **Cu-AD-AA** and **Cu-AD-PA** after the synthesis reaction are shown in Supplementary Figure 2.

X-ray crystallography

Crystallography data of **Cu-AD-FA** was collected at room temperature on a Bruker Apex III CCD single crystal diffractometer by graphite-monochromated Mo-Kα (λ = 0.71073 Å). The structure was solved by a direct method and then refined by a least square method on F^2 in Olex2. The hydrogen atoms were added geometrically. The formula of **Cu-AD-FA** is $Cu_2(AD)_2(FA)_2(DMF)_{1.5}$. The CCDC number of **Cu-AD-FA** is 2312625. Crystal data and structural refinement results are summarized in Supplementary Table 1.

RESULTS AND DISCUSSION

Crystal structure description

By adjusting the size of the terminal ligands in the channel in a unified structure, the channel environment can be effectively improved to achieve a small regulation and a large influence[52,53]. For example, the aqueous synthesis of **MOF-808**, previously reported by our group, improved the water adsorption performance by modifying the carboxylic acid-based modulator, enabling the straightforward tuning of the pore environment[54]. In this study, a classic Bio-MOF platform is utilized, which was composed of AD ligand, Cu^{2+} ions and terminal ligand (FA, AA, PA). It is worth mentioning that similar structures were observed in **Bio-MOF-11-14** series, which consisted of cobalt ions with AD and terminal carboxylic acid ligands. Specifically, **Bio-MOF-11** was isoreticular to **Cu-AD-AA**, and **Bio-MOF-12** was isoreticular to **Cu-AD-PA**[48,49]. It provides significant evidence for the outstanding designability of this series of materials as a reticular chemistry platform. The unit cell parameters for these MOFs can be found in Supplementary Table 2, indicating that as the size of the terminal ligand increases, the unit cell parameters are slightly elongated along the a and b axes but compressed along the c axis. The theoretical pore volumes for the three MOFs are 0.35 (**Cu-AD-FA**), 0.28 (**Cu-AD-AA**), and 0.23 cm^3/g (**Cu-AD-PA**), respectively, due to the increased density of the skeleton.

The structure of **Cu-AD-FA** was determined by single-crystal X-ray structure analysis, and the other two structures were proved by PXRD characterization [Supplementary Figure 3]. The structure of these three Bio-MOFs is illustrated in detail in Figure 1. In Figure 1A, Copper dimer clusters are connected to AD ligands, forming a three-dimensional structure. Each copper dimer is linked by four AD ligands and two monocarboxylic acids. Each AD ligand links to two copper dimers, resulting in one nitrogen atom and one amino group per AD within the structure, which can serve as polar adsorption sites. These MOFs exhibit the same **lvt** topology as the aforementioned MOFs [Supplementary Figure 4A]. However, different terminal ligands cause slight changes within the pore [Figure 1B-D]. The steric hindrance of the terminal ligands gradually transforms the pore size from narrow to more open. To observe this change more directly, Supplementary Figure 4B-D show that the distance between nitrogen atoms and amino groups at the same position increases as the size of the terminal ligands enlarges (3.2 Å for **Cu-AD-FA**, 4.4 Å for **Cu-AD-AA** and 5.4 Å for **Cu-AD-PA**). Instead of conforming to a traditional one-dimensional channel, the structure of this series exhibits three-dimensional intercrossed channels [Figure 1E-G]. Notable alterations occur within the interior environment of the cavity due to variations of the terminal ligands. The inner wall of the channel is non-uniformly smooth; thus, measurements primarily focus on the length of crossed positions and long cavity length. In the **Cu-AD-FA** structure depicted in Figure 1H, there are two dimensions of cavities within the Z-shaped channel: a longer cavity measuring approximately 11.2 Å in length and a narrower cavity with a width of 8.2 Å. Unlike **Cu-AD-FA**, **Cu-AD-AA** incorporates methyl group into its skeleton, which widens the pore size. Consequently, both the long cage and narrower cavity increase to approximately 12.7 Å and 8.8 Å, respectively [Figure 1I]. Notably, more pronounced changes occur with **Cu-AD-PA**, where ethyl group is introduced into the **Cu-AD-FA** structure. While the long cavity size remains around 12.7 Å, the narrow cavity reduces to about 6.8 Å [Figure 1J]. This slight change in the tunnel environment is highly intriguing, prompting us to investigate their adsorption properties concerning light hydrocarbons.

Thermal and chemical stability

The thermal stability of these materials was investigated through TGA analysis and variable temperature PXRD tests [Supplementary Figures 5 and 6]. Variable temperature PXRD tests revealed that **Cu-AD-FA** could withstand temperatures up to 100 °C before its structure collapsed at 150 °C [Supplementary Figure 6A]. Conversely, **Cu-AD-AA** demonstrated good crystallization even at 200 °C, with slight broadening observed at 250 °C and a significant decrease in crystallinity at 300 °C, accompanied by weakened peak intensity [Supplementary Figure 6B]. Similarly, **Cu-AD-PA** showed comparable thermal stability to **Cu-AD-AA**, maintaining strong peak intensity without broadening up to 250 °C but experiencing decreased crystallinity beyond that temperature [Supplementary Figure 6C]. After soaking in different solvents for three days, PXRD tests proved that the three compounds have excellent chemical stability [Supplementary Figure 7]. The water stability test was conducted. After one day of soaking the three MOFs materials in water, the samples were reactivated for nitrogen adsorption measurements. The results show that the water stability of the three materials is not good enough, but their resistance to water is slightly different, among which **Cu-AD-PA** has the strongest resistance to water, followed by **Cu-AD-AA** and **Cu-AD-FA** [Supplementary Figure 8]. These differences can be attributed to the hydrophobicity changes of the terminal ligands.

Porosity of Cu-AD-FA, Cu-AD-AA and Cu-AD-PA

Prior to the 77 K nitrogen adsorption test, these three MOFs underwent pre-activation. Approximately 300 mg of the synthesized sample was placed into a 40 mL centrifuge tube and immersed in EtOH. After a soaking period of four hours, centrifugation was conducted, and the supernatant was discarded. Subsequently, fresh EtOH was added, and the process was repeated. Following an additional two-day exchange period, the solid sample underwent centrifugation, followed by placement in a vacuum oven for

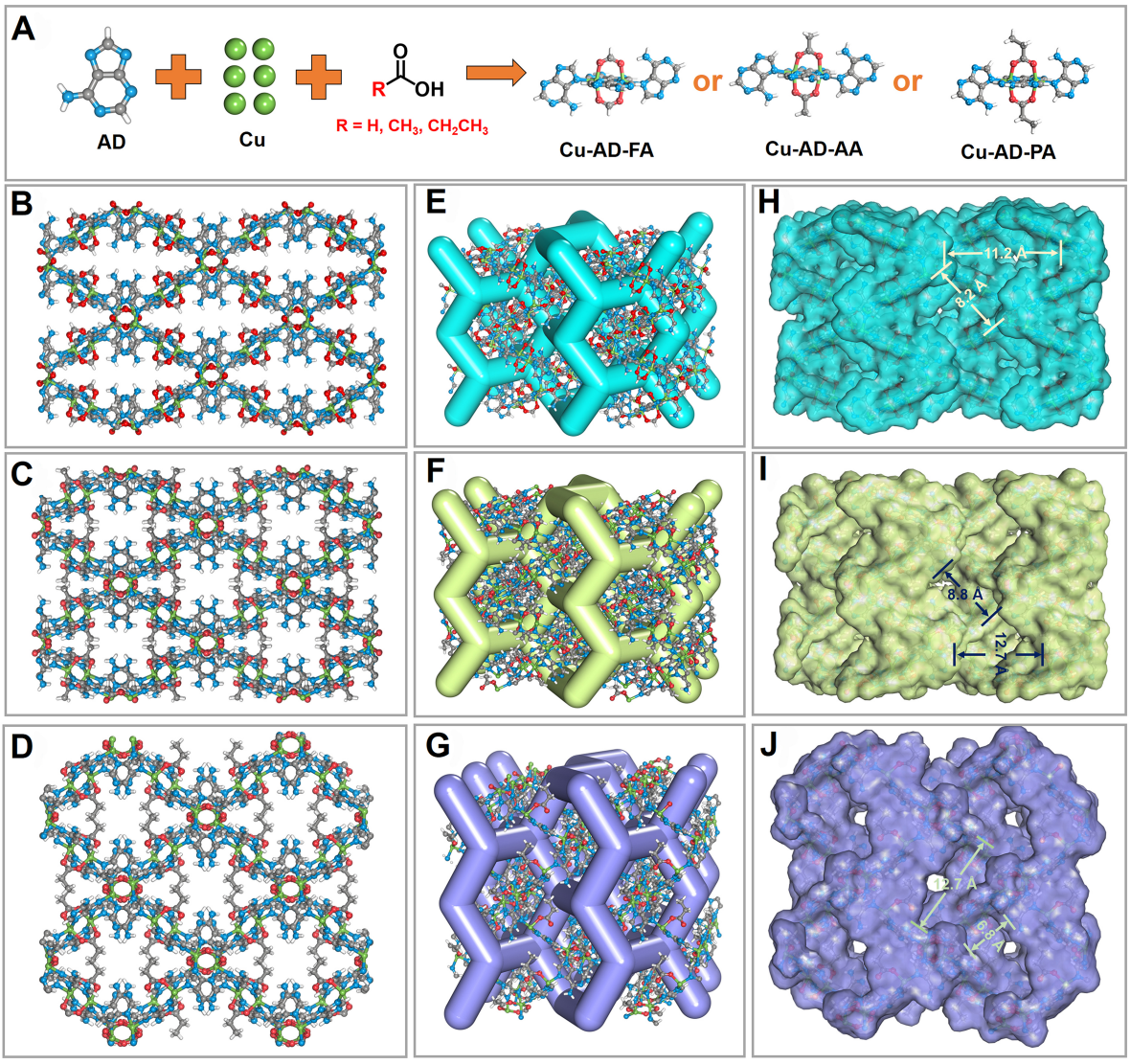

Figure 1. Structure of **Cu-AD-FA**, **Cu-AD-AA** and **Cu-AD-PA**. (A) The composition structure of metal clusters; Ball and stick diagram of (B) **Cu-AD-FA**; (C) **Cu-AD-AA**; and (D) **Cu-AD-PA**. The three-dimensional intercrossed channels of (E) **Cu-AD-FA**; (F) **Cu-AD-AA**; and (G) **Cu-AD-PA**. Pore structure displayed by Connolly surface of (H) **Cu-AD-FA**; (I) **Cu-AD-AA**; and (J) **Cu-AD-PA**. Color scheme. White: Hydrogen; gray: carbon; blue: nitrogen; red: oxygen; green: copper.

degassing at room temperature for 20 min. The dried sample was then transferred to an adsorption tube and subjected to heating and degassing on a Micromeritics ASAP 2420 instrument for ten hours. It is worth noting that there was a slight difference in the pre-treatment temperatures. **Cu-AD-FA** required removal of guest molecules at a temperature of 40 °C, while **Cu-AD-AA** and **Cu-AD-PA** necessitated their removal at a temperature of 90 °C. This discrepancy arises from the poor thermal stability exhibited by **Cu-AD-FA**, as its skeleton tends to collapse with increasing temperature [Supplementary Figure 9].

The resulting 77 K nitrogen adsorption isotherm is depicted in Figure 2A. Among them, **Cu-AD-AA** exhibits the highest adsorption capacity, with its actual pore volume closely aligning with theoretical values. Conversely, **Cu-AD-FA** falls short of reaching its theoretical pore volume due to partial skeleton collapse, whereas **Cu-AD-PA** successfully achieves its theoretical pore volume. Compared to previously reported

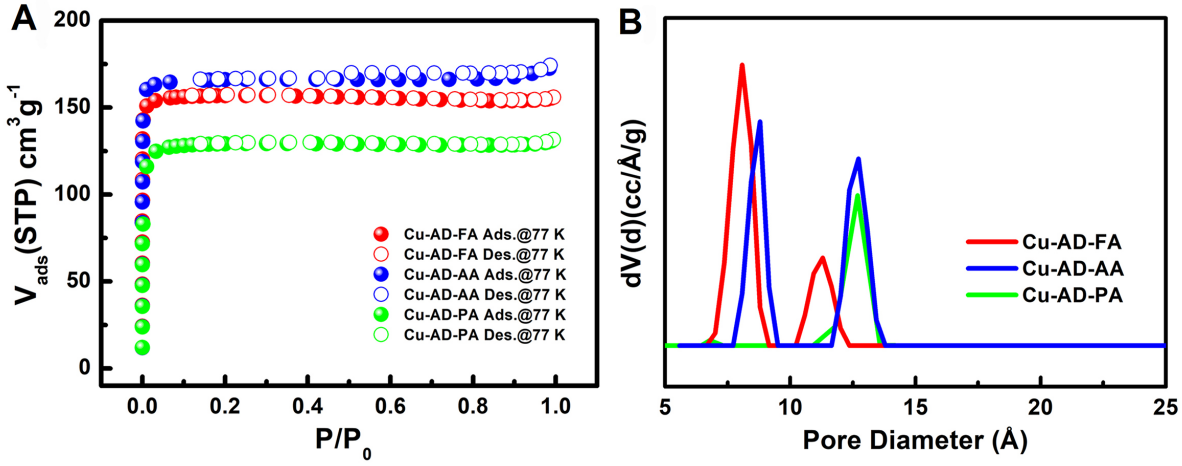

Figure 2. (A) N_2 sorption isotherms for **Cu-AD-FA**, **Cu-AD-AA** and **Cu-AD-PA** at 77 K; (B) The pore size distributions of **Cu-AD-FA**, **Cu-AD-AA** and **Cu-AD-PA** calculated by NLDFT model. NLDFT: Non-local density functional theory.

works[49], the three materials synthesized via solvothermal synthesis in this study show significantly fewer defects and notable improvements in pore volume and Brunauer-Emmett-Teller (BET) specific surface area [Table 1], indicating that these MOFs materials in this work are more suitable for gas adsorption and separation investigation. The pore size distributions of **Cu-AD-FA**, **Cu-AD-AA** and **Cu-AD-PA** calculated by the nonlocal density functional theory (NLDFT) model, which are basically consistent with the dimensions measured by the crystal structure [Figure 2B]. The pore volume and thermal stability of these three materials exhibit a remarkable trade-off effect. Specifically, **Cu-AD-AA** demonstrates optimal properties, displaying enhanced stability and a high BET specific surface area.

Gas adsorption behavior of Cu-AD-FA, Cu-AD-AA and Cu-AD-PA

To comprehensively elucidate the impact of pore microenvironment changes on gas adsorption properties, adsorption isotherms of CO_2 and C_1-C_3 light hydrocarbon gas molecules were tested at 273 and 298 K, respectively [Supplementary Figures 10-13]. In order to more clearly describe the adsorption properties of these MOFs materials, the adsorption isotherms at 298 K and their adsorption enthalpies (Q_{st}) were shown in Figure 3. The adsorption capacity of C_3 and C_2 molecules for the three MOFs is significantly higher than that of CH_4 [Figure 3A-C]. This discrepancy stems from the greater polarizability and larger molecular size of C_2 and C_3, facilitating stronger interactions with the framework [Supplementary Table 3]. Notably, the variance in adsorption capacity is most pronounced at low pressures. Detailed specific adsorption values at 10 kPa and 101 kPa at 298 K can be found in Supplementary Table 4. Regarding C_2 molecules, the presence of polar sites within the pores plays a crucial role in their binding ability. In terms of a horizontal comparison, C_2H_2 possesses the smallest pKa value and can form hydrogen bonds with numerous amino and nitrogen atoms within the pores, leading to higher adsorption capacity than C_2H_4 and C_2H_6. C_2H_4 and C_2H_6 exhibit similar sizes and polarities, consequently resulting in comparable adsorption capacities. From a longitudinal perspective, the channel environment undergoes minimal changes from **Cu-AD-FA** to **Cu-AD-AA** and then to **Cu-AD-PA**, yet these modifications significantly influence the adsorption capacity of C_2 molecules. Specifically, the adsorption capacity of **Cu-AD-FA** for C_2H_2 at 10 and 101 kPa is merely 18 and 42 cm^3/g, while under the same conditions, the adsorption capacity of **Cu-AD-AA** for C_2H_2 reaches as high as 32 cm^3/g and 67 cm^3/g. Clearly, besides the role of the amino group, the dispersion force between methyl and C_2H_2 also contributes positively. The adsorption capacity of **Cu-AD-PA** for C_2H_2 is 29 and 60 cm^3/g, which may explain the lower pore volume compared to **Cu-AD-AA**, although it still surpasses the

Table 1. BET surface area, Langmuir surface area, pore volume measured by experiment, theoretical pore volume and comparison of pore volume reported in the literature[49]

MOFs	BET (m^2/g)	Langmuir (m^2/g)	Pore volume (cm^3/g)	Theoretical pore volume (cm^3/g)	Reference pore volume (cm^3/g)
Cu-AD-FA	650	672	0.24	0.35	-
Cu-AD-AA	712	754	0.27	0.28	0.17
Cu-AD-PA	662	688	0.20	0.23	0.11

BET: Brunauer-Emmett-Teller; MOFs: metal–organic frameworks.

adsorption capacity of **Cu-AD-FA**. Similarly, under analogous conditions, the adsorption capacities of C_2H_4 and C_2H_6 follow a similar gradient trend, with **Cu-AD-AA** exceeding both **Cu-AD-PA** and **Cu-AD-FA**. Similar to the C_2 molecule, the adsorption capacity of **Cu-AD-FA** for the C_3 molecule remains the lowest among the three. The adsorption capacity of **Cu-AD-PA** for C_3 molecules is inferior to that of **Cu-AD-AA**, possibly due to a reduction in pore volume and the free rotation of the ethyl group. At 298 K, 1 bar, the C_3H_8 adsorption capacities of the three MOFs were 21 (**Cu-AD-FA**), 74 (**Cu-AD-AA**) and 33 cm^3/g (**Cu-AD-PA**), respectively. Under the same conditions, the adsorption capacities for C_3H_6 were 21, 75 and 37 cm^3/g, respectively. Notably, **Cu-AD-AA** demonstrates a remarkable adsorption capacity for C_3H_6, with an adsorption amount of 59 cm^3/g at 10 kPa and 298 K, surpassing several high-performance C_3H_6 adsorbents such as nickel nitroprusside (Ni-NP)[55], NUM-7a (an ultramicroporous Mn-based MOF)[56], NKMOF-11 (a new ultramicroporous MOF)[57], and hydrogen-bonded organic framework (HOF)-16a[58]. Additionally, **Cu-AD-AA** also exhibits significant C_3H_8 uptake (56 cm^3/g) at 10 kPa. Clearly, the internal environment of the **Cu-AD-AA** channel facilitates the adsorption of C_3 molecules. In terms of CO_2 adsorption, **Cu-AD-AA** demonstrated the highest adsorption capacity among the three materials, reaching 65.45 cm^3/g at 298 K and 1 bar. **Cu-AD-FA** exhibited a slightly lower adsorption capacity of 58.44 cm^3/g, while **Cu-AD-PA** displayed the lowest adsorption capacity at 28.72 cm^3/g.

To assess the interaction strength between the host framework and these light hydrocarbons and CO_2, the adsorption enthalpies for the three MOFs were calculated. The Virial equation was employed to fit the adsorption curves at 273 K and 298 K, from which the Q_{st} values were derived [Supplementary Figures 14-17]. As depicted in Figure 3D, the Q_{st} values of **Cu-AD-FA** for various gases are as follows: CO_2 (28.3 kJ/mol), CH_4 (15.7 kJ/mol), C_2H_2 (24.8 kJ/mol), C_2H_4 (21.7 kJ/mol), C_2H_6 (21.3 kJ/mol), C_3H_6 (25.1 kJ/mol), and C_3H_8 (24.2 kJ/mol). In contrast, **Cu-AD-AA** exhibits significantly higher Q_{st} for C_3H_6 (48.7 kJ/mol) and C_3H_8 (43.1 kJ/mol) compared to CH_4 (16.4 kJ/mol). Additionally, the Q_{st} of **Cu-AD-AA** for CO_2, C_2H_2, C_2H_4, and C_2H_6 are 25.87, 34.2, 32.0, and 29.9 kJ/mol, respectively [Figure 3E]. On the other hand, **Cu-AD-PA** shows the following Q_{st} for various gases: CO_2 (16.83 kJ/mol), CH_4 (15.1 kJ/mol), C_2H_2 (32.7 kJ/mol), C_2H_4 (28.2 kJ/mol), C_2H_6 (26.9 kJ/mol), C_3H_6 (27.8 kJ/mol), and C_3H_8 (26.3 kJ/mol) [Figure 3F]. A clear comparison reveals that **Cu-AD-AA** demonstrates a stronger affinity towards C_3 and C_2 molecules, while **Cu-AD-FA** exhibits the weakest affinity for these specific gas molecules. Based on these findings, it is evident that **Cu-AD-AA** holds the highest potential for effectively separating natural gas and MTO product.

Gas separation behavior of Cu-AD-FA, Cu-AD-AA and Cu-AD-PA

As illustrated in Supplementary Figures 18-20, the adsorption data (CO_2, CH_4, C_2H_2, C_2H_4, C_2H_6, C_3H_6, and C_3H_8) obtained from experiments for **Cu-AD-FA**, **Cu-AD-AA**, and **Cu-AD-PA** were fitted using the dual-site Langmuir-Freundlich equation. The fitting parameters are within the error range and are listed in Supplementary Tables 5-7. The theoretical selectivity of **Cu-AD-FA**, **Cu-AD-AA**, and **Cu-AD-PA** for C_2H_2/CH_4, C_2H_4/CH_4, C_2H_6/CH_4, and C_3H_8/CH_4 was predicted by ideal adsorbed solution theory (IAST) calculations. The selectivity for C_3H_8/CH_4 (0.5:0.5) was found to be 36, 746, and 31 for **Cu-AD-FA**,

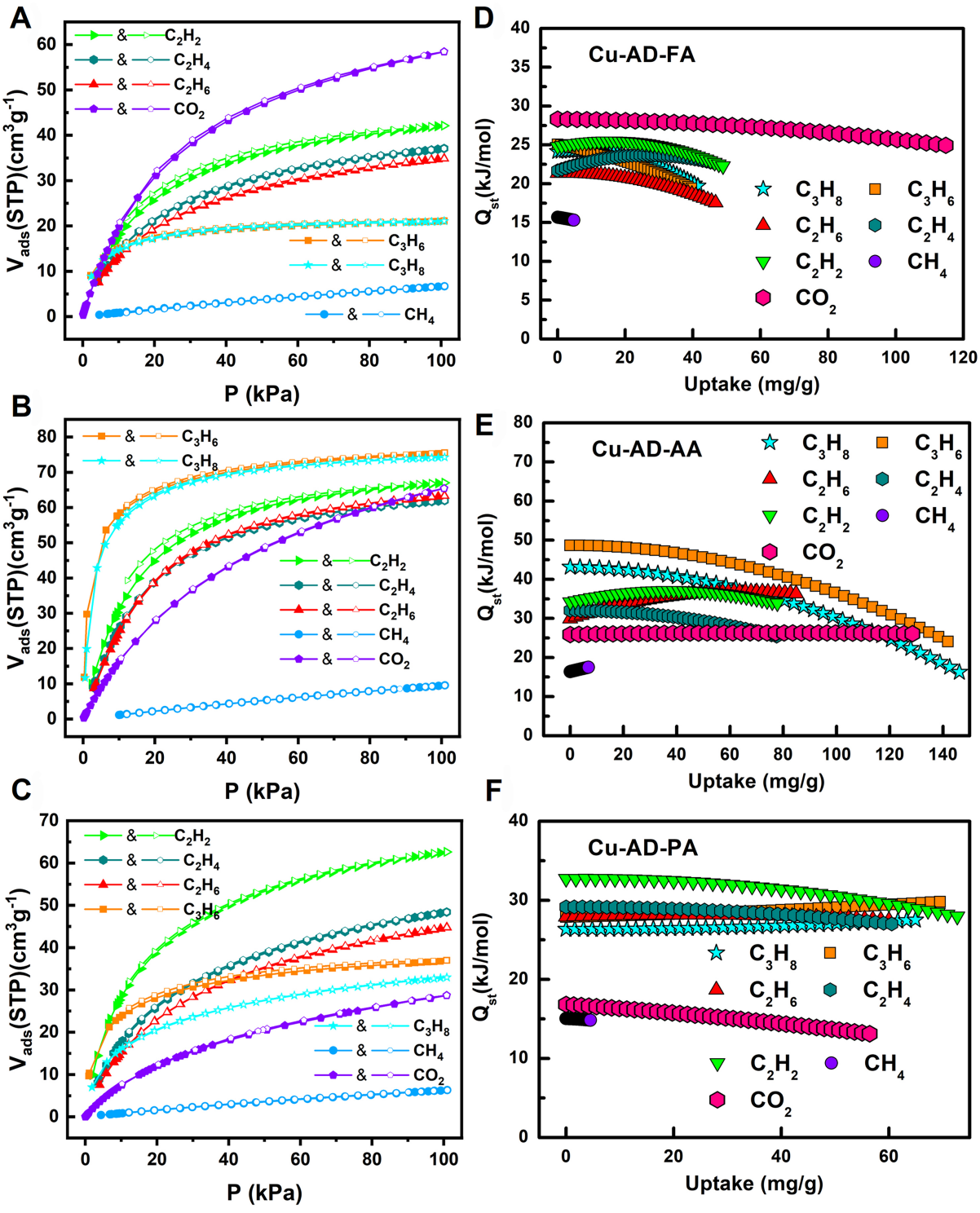

Figure 3. CO_2, CH_4, C_2H_2, C_2H_4, C_2H_6, C_3H_6 and C_3H_8 adsorption isotherms of (A) **Cu-AD-FA**; (B) **Cu-AD-AA**; (C) **Cu-AD-PA** at 298 K and 1 bar. Q_{st} curves of (D) **Cu-AD-FA**; (E) **Cu-AD-AA**; (F) **Cu-AD-PA**.

Cu-AD-AA, and Cu-AD-PA, respectively [Figure 4A]. For C_2H_6/CH_4 (0.5:0.5), the selectivity was 29, 50,

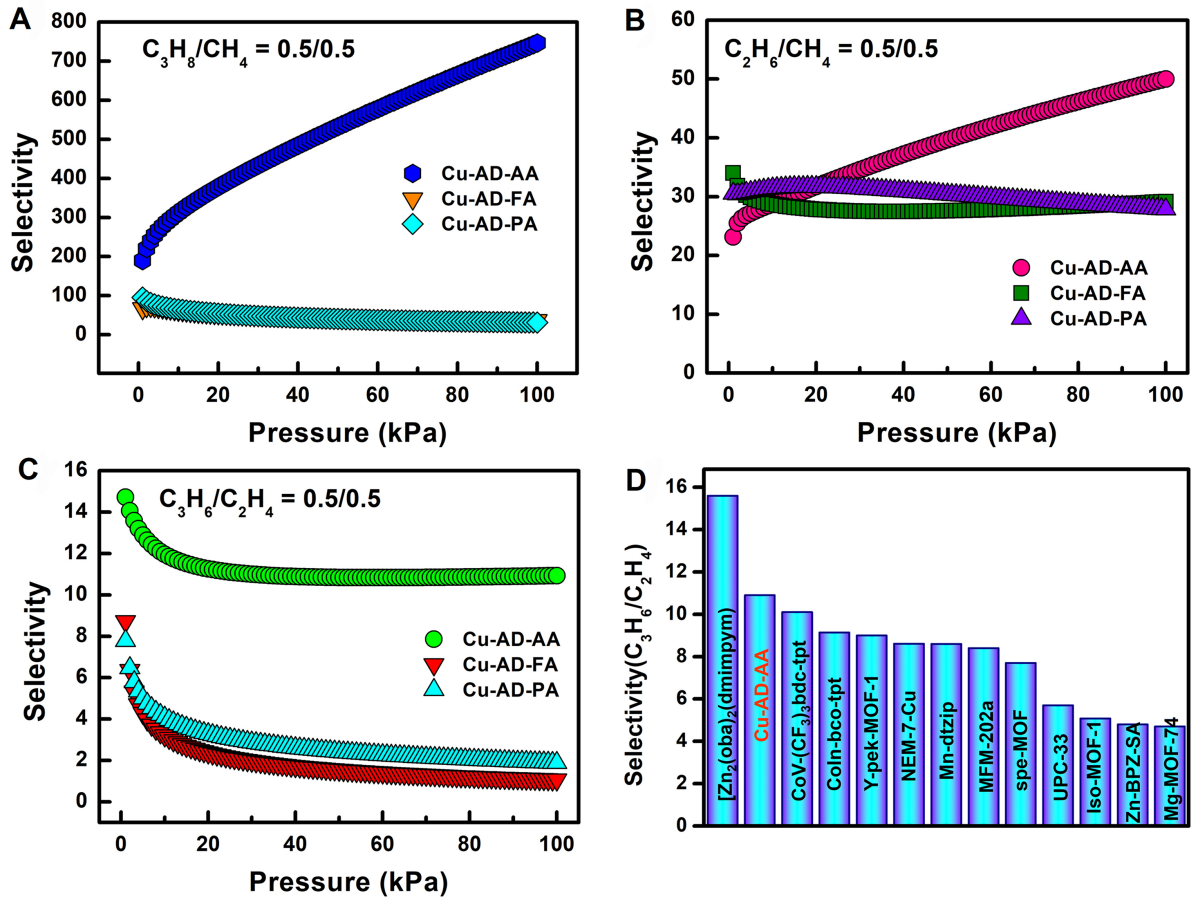

Figure 4. (A) Selectivity of equimolar mixtures of C_3H_8 over CH_4 for **Cu-AD-FA**, **Cu-AD-AA** and **Cu-AD-PA**; (B) Selectivity of equimolar mixtures of C_2H_6 over CH_4 for **Cu-AD-FA**, **Cu-AD-AA** and **Cu-AD-PA**; (C) Selectivity of equimolar mixtures of C_3H_6 over C_2H_4 for **Cu-AD-FA**, **Cu-AD-AA** and **Cu-AD-PA**; (D) Comparison of IAST selectivity of C_3H_6/C_2H_4 (0.5/0.5) with other reported MOFs. IAST: Ideal adsorbed solution theory; MOFs: metal–organic frameworks.

and 28, respectively [Figure 4B]. Similarly, for C_2H_2/CH_4 (0.5:0.5), the selectivity was 53, 81, and 68 for **Cu-AD-FA**, **Cu-AD-AA**, and **Cu-AD-PA**, respectively, and for C_2H_4/CH_4 (0.5:0.5), the selectivity was 34, 54, and 34 [Supplementary Figure 21]. Notably, **Cu-AD-AA** exhibits higher selectivity for C_3H_8/CH_4 and C_2H_6/CH_4 than many previously reported famous MOFs. **Cu-AD-AA** demonstrated higher selectivity for C_3H_8/CH_4 compared to ZUL-C2 (632)[59], PCN-224 (609)[60], FJI-C1 (471)[61] and BSF-1 (353)[62]. The selectivity of **Cu-AD-AA** for C_2H_6/CH_4 is lower than that of top-performing MOFs such as ZUL-C2 (91) and BSF-2 (53)[63]. However, it remains greater than the selectivity of most reported MOFs materials. In summary, **Cu-AD-AA** demonstrates excellent potential as a physical adsorbent for CH_4 purification, given its high selectivity towards C_3H_8/CH_4 and C_2H_6/CH_4. A more detailed comparison of C_3H_8/CH_4 and C_2H_6/CH_4 is found in Supplementary Table 8. Furthermore, the separation selectivity for gas molecules with similar sizes, such as C_2H_2/CO_2, C_2H_4/C_2H_6, and C_3H_6/C_3H_8, was investigated. For C_2H_2/CO_2, it is interesting that **Cu-AD-FA** is preferred for CO_2 adsorption; **Cu-AD-AA** and **Cu-AD-PA** are preferred for C_2H_2 adsorption. The selectivity of CO_2/C_2H_2 (0.5:0.5) for **Cu-AD-FA** is 1.47 and selectivity of C_2H_2/CO_2 (0.5:0.5) for **Cu-AD-AA** and **Cu-AD-PA** are 2.10 and 8.86, respectively [Supplementary Figure 22]. Both C_2H_2/CO_2 selectivity and C_2H_2 adsorption capacity of **Cu-AD-PA** are higher than those synthesized by the diffusion method in the literature, demonstrating the significance of this study once again. The selectivity of **Cu-AD-FA**, **Cu-AD-AA** and **Cu-AD-PA** for C_2H_4/C_2H_6 (0.5:0.5) is 1.16, 1.04 and 1.27, respectively. Their

C_3H_6/C_3H_8 (0.5:0.5) selectivity is 1.53, 1.64 and 3.16, respectively [Supplementary Figure 23].

The selectivity for the separation of MTO product was also determined using IAST calculations [Figure 4C and Supplementary Figure 24]. Supplementary Figures 18 and 20 illustrate the adsorption capacities of C_3H_6 for **Cu-AD-FA** and **Cu-AD-PA**, which are initially higher than those of C_2H_4 at low pressures. However, the adsorption capacity of C_2H_4 surpasses that of C_3H_6 shortly thereafter. Consequently, these MOFs are unsuitable for effectively separating the C_3H_6/C_2H_4 mixture. In contrast, **Cu-AD-AA** exhibits a higher adsorption capacity for C_3H_6 compared to C_2H_4 in both low and high pressure regions [Supplementary Figure 19]. The IAST results presented in Figure 4C and Supplementary Figure 24 indicate that **Cu-AD-AA** demonstrates selectivity values of 10.9 (v/v = 0.1/0.9), 10.8 (v/v = 0.2/0.5), and 10.9 (v/v = 0.5/0.5) for different proportions of C_3H_6/C_2H_4. Conversely, the equimolar selectivity of **Cu-AD-FA** and **Cu-AD-PA** decreases to 1.1 and 1.9 at 101 kPa, indicating their inability to effectively separate C_3H_6 and C_2H_4. Notably, the C_3H_6/C_2H_4 selectivity of **Cu-AD-AA** exceeds that of numerous reported materials. As shown in Figure 4D, the selectivity of **Cu-AD-AA** ranks second, only surpassed by $Zn_2(oba)_2(dmimpym)$ (15.6)[64], and is higher than those reported same type MOFs materials, such as CoV-$(CF_3)_3$bdc-tpt (10.1)[65], Y-pek-MOF-1 (9.0)[15], NEM-7-Cu (8.61)[66], Mn-dtzip (8.6)[67], spe-MOF (7.7)[16] and Zn-BPZ-SA (4.8)[36]. A more detailed comparison is listed in Supplementary Table 9.

Among the three MOFs, **Cu-AD-AA** has the best adsorption capacity and the highest selectivity, achieving a balance between adsorption capacity and selectivity. To assess **Cu-AD-AA** practical separation capability, dynamic breakthrough experiments were conducted at 298 K and 1 bar. Figure 5A illustrates the breakthrough of a gas mixture with a C_3H_8/CH_4 ratio of 50/50 (flow rate: 2 mL/min). Over time, CH_4 rapidly elutes from the column while C_3H_8 remains retained. Calculations indicate that a single breakthrough experiment yields high-purity CH_4 at 1.25 mmol/g. Similarly, Figure 5B demonstrates that after the passage of a C_2H_6/CH_4 gas mixture (50/50, 2 mL/min), CH_4 breaks through first, followed by C_2H_6 after a certain period. The calculated CH_4 yield is 0.22 mmol/g. These results indicate that **Cu-AD-AA** possesses exceptional natural gas purification capabilities.

For MTO product separation, a mixture of C_2H_4:C_3H_6 was introduced into activated **Cu-AD-AA** samples packed in a column at flow rates of 2.0, 4.0, and 5.0 mL/min with ratios of 50:50 [Figure 5C], 50:20 [Figure 5D], and 90:10 [Supplementary Figure 25], respectively. The observations demonstrated that **Cu-AD-AA** effectively separated C_2H_4 and C_3H_6 mixtures, with preferential breakthrough of C_2H_4, while C_3H_6 eluted at 25, 14, and 13 min/g, respectively. Additionally, based on the breakthrough curves, the adsorption amounts of C_3H_6 by **Cu-AD-AA** from the mentioned C_2H_4 and C_3H_6 (50:50, 50:20, and 90:10) mixtures during a single breakthrough period were calculated to be 29.5, 12.1, and 8.2 $cm^3 \cdot g^{-1}$, correspondingly. Moreover, the breakthrough experiments were reproducible in at least three consecutive cycles with regeneration conditions involving vacuum or room temperature helium sweep. This repeatability aligns with its low Q_{st} value, indicating high stability and durability. The stability of **Cu-AD-AA** was maintained after cycle tests, as evidenced by the PXRD analysis [Supplementary Figure 26]. **Cu-AD-AA** demonstrates desirable traits such as high thermal and chemical stability, elevated C_3H_6 absorption rate, and C_2H_4 selectivity, reducing energy consumption during the regeneration process. Consequently, it presents as a promising material for industrial MTO product separation.

CONCLUSIONS

In this study, three AD-based Bio-MOFs were successfully synthesized using a solvothermal method, employing monocarboxylic acids with varying sizes as coordinated terminal ligands. These MOFs exhibited distinct pore microenvironments arising from differences in terminal ligand sizes. Systematic investigation

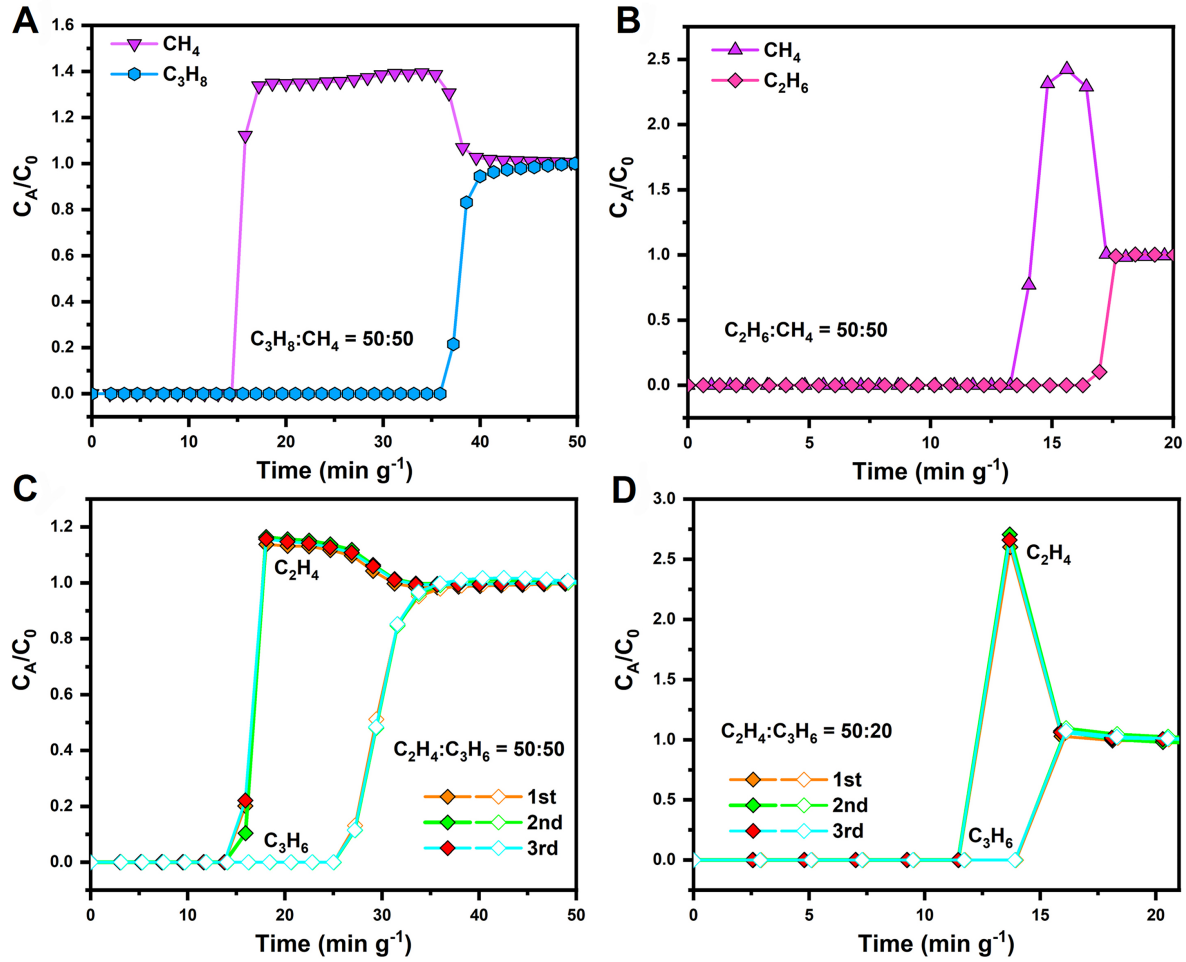

Figure 5. The breakthrough curves of the (A) C_3H_8/CH_4 mixtures (v/v = 50/50 under a flow of 2 mL/min); (B) C_2H_6/CH_4 mixtures (v/v = 50/50 under a flow of 2 mL/min); (C) C_2H_4/C_3H_6 mixtures (v/v = 50/50 under a flow of 2 mL/min); (D) C_2H_4/C_3H_6 mixtures (v/v = 50/20 under a flow of 4 mL/min) in an absorber bed packed with **Cu-AD-AA** at 298 K and 1 bar.

revealed a significant enhancement of thermal stability with larger terminal ligands. Furthermore, evaluation of their adsorption properties for light hydrocarbons revealed diverse capacities for adsorption and selective separation, attributable to their three-dimensional intercrossed channels and abundant active sites within. As a result, it demonstrated their aptitude for adsorbing $C_3 > C_2 > C_1$ molecules, making them suitable for natural gas purification and MTO product separation. Qualitative analysis through IAST further confirmed the potential of these Bio-MOFs in CH_4 purification and MTO product separation, with **Cu-AD-AA** exhibiting the most favorable separation properties. Quantification of separation ability was corroborated by dynamic breakthrough experiments. The inferior adsorption and separation capacity of **Cu-AD-FA** can be attributed to its poor stability and limited active sites compared to **Cu-AD-AA**. Although **Cu-AD-PA** demonstrated greater stability than **Cu-AD-AA**, its reduced pore volume and unrestricted rotation of ethyl groups within the pores contributed to significantly poorer adsorption and separation capabilities. The subtle variations in small channel environments among the three materials presented intriguing trade-offs, including the balance between high adsorption capacity and selectivity and the relationship between pore volume and stability. Based on the current findings, **Cu-AD-AA** appears to strike a favorable balance within these trade-offs, considering stability, adsorption capacity, and selectivity. It presents an encouraging prospect for designing separation materials with superior performance.

Furthermore, the bio-based nature of **Cu-AD-AA**, coupled with its low toxicity and cost-effectiveness, further highlights the significance of this study. Combined with its straightforward synthesis method and robust separation capabilities, **Cu-AD-AA** exhibits substantial potential for various industrial applications.

DECLARATIONS

Authors' contributions

Provided financial support: Liu Y
Revised and finalized the manuscript: Liu Y, Zhang L
Designed the samples, performed experiments, and wrote the paper: Liu Y, Li W, Zhang L
Offered the experimental guidance and advice: Xue D
Assisted with data supplement: Wang Y, Wang D, Shi Z, Liu J
All authors contributed to the general discussion.

Availability of data and materials

Not applicable.

Financial support and sponsorship

This work was supported by the National Natural Science Foundation of China (Nos. 22171100 and U23A20360) and the 111 Project (B17020).

Conflicts of interest

All authors declared that there are no conflicts of interest.

Ethical approval and consent to participate

Not applicable.

Consent for publication

Not applicable.

REFERENCES

1. Yang Y, Li L, Lin RB, et al. Ethylene/ethane separation in a stable hydrogen-bonded organic framework through a gating mechanism. *Nat Chem* 2021;13:933-9. DOI
2. Jiang Y, Hu Y, Luan B, et al. Benchmark single-step ethylene purification from ternary mixtures by a customized fluorinated anion-embedded MOF. *Nat Commun* 2023;14:401. DOI PubMed PMC
3. Fan W, Ying Y, Peh SB, et al. Multivariate polycrystalline metal–organic framework membranes for CO_2/CH_4 separation. *J Am Chem Soc* 2021;143:17716-23. DOI PubMed
4. Zhang Z, Deng Z, Evans HA, et al. Exclusive recognition of CO_2 from hydrocarbons by aluminum formate with hydrogen-confined pore cavities. *J Am Chem Soc* 2023;145:11643-9. DOI PubMed
5. Ryckebosch E, Drouillon M, Vervaeren H. Techniques for transformation of biogas to biomethane. *Biomass Bioenerg* 2011;35:1633-45. DOI
6. Li L, Lin RB, Krishna R, et al. Ethane/ethylene separation in a metal–organic framework with iron-peroxo sites. *Science* 2018;362:443-6. DOI
7. Liu Y, Chen Z, Liu G, et al. Conformation-controlled molecular sieving effects for membrane-based propylene/propane separation. *Adv Mater* 2019;31:e1807513. DOI PubMed
8. Zhang Y, Xiao H, Zhou X, Wang X, Li Z. Selective adsorption performances of UiO-67 for separation of light hydrocarbons C1, C2, and C3. *Ind Eng Chem Res* 2017;56:8689-96. DOI
9. Han XH, Gong K, Huang X, et al. Syntheses of covalent organic frameworks via a one-pot suzuki coupling and schiff's base reaction for C_2H_4/C_3H_6 separation. *Angew Chem Int Ed Engl* 2022;61:e202202912. DOI PubMed

10. Tian P, Wei Y, Ye M, Liu Z. Methanol to olefins (MTO): from fundamentals to commercialization. *ACS Catal* 2015;5:1922-38. DOI
11. Chen Y, Yang Y, Wang Y, et al. Ultramicroporous hydrogen-bonded organic framework material with a thermoregulatory gating effect for record propylene separation. *J Am Chem Soc* 2022;144:17033-40. DOI
12. Chen KJ, Madden DG, Mukherjee S, et al. Synergistic sorbent separation for one-step ethylene purification from a four-component mixture. *Science* 2019;366:241-6. DOI
13. Liu Y, Liu J, Xiong H, et al. Negative electrostatic potentials in a Hofmann-type metal–organic framework for efficient acetylene separation. *Nat Commun* 2022;13:5515. DOI PubMed PMC
14. Peng YL, Wang T, Jin C, et al. Efficient propyne/propadiene separation by microporous crystalline physiadsorbents. *Nat Commun* 2021;12:5768. DOI PubMed PMC
15. Wei W, Guo X, Zhang Z, Zhang Y, Xue D. Topology-guided synthesis and construction of amide-functionalized rare-earth metal–organic frameworks. *Inorg Chem Commun* 2021;133:108896. DOI
16. Fang H, Zheng B, Zhang ZH, Li HX, Xue DX, Bai J. Ligand-conformer-induced formation of zirconium-organic framework for methane storage and MTO product separation. *Angew Chem Int Ed Engl* 2021;60:16521-8. DOI PubMed
17. Gao S, Morris CG, Lu Z, et al. Selective hysteretic sorption of light hydrocarbons in a flexible metal–organic framework material. *Chem Mater* 2016;28:2331-40. DOI
18. Hiraide S, Sakanaka Y, Kajiro H, Kawaguchi S, Miyahara MT, Tanaka H. High-throughput gas separation by flexible metal–organic frameworks with fast gating and thermal management capabilities. *Nat Commun* 2020;11:3867. DOI PubMed PMC
19. Fan W, Zhang X, Kang Z, Liu X, Sun D. Isoreticular chemistry within metal–organic frameworks for gas storage and separation. *Coord Chem Rev* 2021;443:213968. DOI
20. Li J, Bhatt PM, Li J, Eddaoudi M, Liu Y. Recent progress on microfine design of metal–organic frameworks: structure regulation and gas sorption and separation. *Adv Mater* 2020;32:e2002563. DOI PubMed
21. Hu P, Hu J, Liu H, et al. Quasi-orthogonal configuration of propylene within a scalable metal–organic framework enables its purification from quinary propane dehydrogenation byproducts. *ACS Cent Sci* 2022;8:1159-68. DOI PubMed PMC
22. Zeng H, Xie M, Wang T, et al. Orthogonal-array dynamic molecular sieving of propylene/propane mixtures. *Nature* 2021;595:542-8. DOI
23. Long JR, Yaghi OM. The pervasive chemistry of metal–organic frameworks. *Chem Soc Rev* 2009;38:1213-4. DOI PubMed
24. Zhou HC, Long JR, Yaghi OM. Introduction to metal–organic frameworks. *Chem Rev* 2012;112:673-4. DOI PubMed
25. Zheng F, Chen R, Ding Z, et al. Interlayer symmetry control in flexible-robust layered metal–organic frameworks for highly efficient C_2H_2/CO_2 separation. *J Am Chem Soc* 2023;145:19903-11. DOI PubMed
26. Gulati S, Vijayan S, Mansi, et al. Recent advances in the application of metal–organic frameworks (MOFs)-based nanocatalysts for direct conversion of carbon dioxide (CO_2) to value-added chemicals. *Coord Chem Rev* 2023;474:214853. DOI
27. Li L, Jung HS, Lee JW, Kang YT. Review on applications of metal–organic frameworks for CO_2 capture and the performance enhancement mechanisms. *Renew Sust Energy Rev* 2022;162:112441. DOI
28. Yang S, Hu T. Reverse-selective metal–organic framework materials for the efficient separation and purification of light hydrocarbons. *Coord Chem Rev* 2022;468:214628. DOI
29. Xie Y, Shi Y, Cedeño Morales EM, et al. Optimal binding affinity for sieving separation of propylene from propane in an oxyfluoride anion-based metal–organic framework. *J Am Chem Soc* 2023;145:2386-94. DOI PubMed
30. Deneff JI, Rohwer LES, Butler KS, et al. Orthogonal luminescence lifetime encoding by intermetallic energy transfer in heterometallic rare-earth MOFs. *Nat Commun* 2023;14:981. DOI PubMed PMC
31. Liu Q, Wu B, Li M, Huang Y, Li L. Heterostructures made of upconversion nanoparticles and metal–organic frameworks for biomedical applications. *Adv Sci* 2022;9:e2103911. DOI PubMed PMC
32. Hashjin M, Zarshad S, Motejadded Emrooz HB, Sadeghzadeh S. Enhanced atmospheric water harvesting efficiency through green-synthesized MOF-801: a comparative study with solvothermal synthesis. *Sci Rep* 2023;13:16983. DOI PubMed PMC
33. Shi L, Li N, Wang D, Fan M, Zhang S, Gong Z. Environmental pollution analysis based on the luminescent metal organic frameworks: a review. *TrAC Trend Anal Chem* 2021;134:116131. DOI
34. Lin JY. CHEMISTRY. Molecular sieves for gas separation. *Science* 2016;353:121-2. DOI PubMed
35. Datta SJ, Mayoral A, Murthy Srivatsa Bettahalli N, et al. Rational design of mixed-matrix metal–organic framework membranes for molecular separations. *Science* 2022;376:1080-7. DOI
36. Wang G, Krishna R, Li Y, et al. Rational construction of ultrahigh thermal stable MOF for efficient separation of MTO products and natural gas. *ACS Mater Lett* 2023;5:1091-9. DOI
37. Dong Q, Huang Y, Hyeon-deuk K, et al. Shape- and size-dependent kinetic ethylene sieving from a ternary mixture by a trap-and-flow channel crystal. *Adv Funct Mater* 2022;32:2203745. DOI
38. Yaghi OM. Reticular chemistry-construction, properties, and precision reactions of frameworks. *J Am Chem Soc* 2016;138:15507-9. DOI PubMed
39. Ke T, Wang Q, Shen J, et al. Molecular sieving of C_2-C_3 alkene from alkyne with tuned threshold pressure in robust layered metal–organic frameworks. *Angew Chem Int Ed Engl* 2020;59:12725-30. DOI
40. Eddaoudi M, Kim J, Rosi N, et al. Systematic design of pore size and functionality in isoreticular MOFs and their application in methane storage. *Science* 2002;295:469-72. DOI
41. Pei J, Wang J, Shao K, et al. Engineering microporous ethane-trapping metal–organic frameworks for boosting ethane/ethylene

separation. *J Mater Chem A* 2020;8:3613-20. DOI

42. Meng SS, Xu M, Guan H, et al. Anisotropic flexibility and rigidification in a TPE-based Zr-MOFs with scu topology. *Nat Commun* 2023;14:5347. DOI PubMed PMC
43. Lyu H, Chen OI, Hanikel N, et al. Carbon dioxide capture chemistry of amino acid functionalized metal–organic frameworks in humid flue gas. *J Am Chem Soc* 2022;144:2387-96. DOI
44. Zulys A, Yulia F, Muhadzib N, Nasruddin. Biological metal–organic frameworks (Bio-MOFs) for CO_2 capture. *Ind Eng Chem Res* 2021;60:37-51. DOI
45. Binaeian E, Nabipour H, Ahmadi S, Rohani S. The green synthesis and applications of biological metal–organic frameworks for targeted drug delivery and tumor treatments. *J Mater Chem B* 2023;11:11426-59. DOI
46. Si Y, Luo H, Zhang P, et al. CD-MOFs: from preparation to drug delivery and therapeutic application. *Carbohydr Polym* 2024;323:121424. DOI
47. Wang L, Lv J, Ye Q, Luo Y, Wang G, Xie L. Nanoporous Cu(II)-adenine-based metal–organic frameworks for selective adsorption of C_2H_2 from C_2H_4 and CO_2. *ACS Appl Nano Mater* 2023;6:22095-103. DOI
48. Li T, Chen D, Sullivan JE, Kozlowski MT, Johnson JK, Rosi NL. Systematic modulation and enhancement of CO_2:N_2 selectivity and water stability in an isoreticular series of bio-MOF-11 analogues. *Chem Sci* 2013;4:1746-55. DOI
49. Pérez-Yáñez S, Beobide G, Castillo O, et al. Open-framework copper adeninate compounds with three-dimensional microchannels tailored by aliphatic monocarboxylic acids. *Inorg Chem* 2011;50:5330-2. DOI
50. Pérez-yáñez S, Beobide G, Castillo O, et al. Gas adsorption properties and selectivity in Cu^{II}/adeninato/carboxylato metal–biomolecule frameworks. *Eur J Inorg Chem* 2012;2012:5921-33. DOI
51. Li H, Bonduris H, Zhang X, et al. A microporous metal–organic framework with basic sites for efficient C_2H_2/CO_2 separation. *J Solid State Chem* 2020;284:121209. DOI
52. Song C, Zheng F, Liu Y, et al. Spatial distribution of nitrogen binding sites in metal–organic frameworks for selective ethane adsorption and one-step ethylene purification. *Angew Chem Int Ed Engl* 2023;62:e202313855. DOI
53. Chen OIF, Liu CH, Wang K, et al. Water-enhanced direct air capture of carbon dioxide in metal–organic frameworks. *J Am Chem Soc* 2024;146:2835-44. DOI
54. Liu X, Kirlikovali KO, Chen Z, et al. Small molecules, big effects: tuning adsorption and catalytic properties of metal–organic frameworks. *Chem Mater* 2021;33:1444-54. DOI
55. Xie Y, Shi Y, Cui H, Lin R, Chen B. Efficient separation of propylene from propane in an ultramicroporous cyanide-based compound with open metal sites. *Small Struct* 2022;3:2100125. DOI
56. Yang SQ, Sun FZ, Krishna R, et al. Propane-trapping ultramicroporous metal–organic framework in the low-pressure area toward the purification of propylene. *ACS Appl Mater Interfaces* 2021;13:35990-6. DOI
57. Peng Y, Wang T, Jin C, et al. A robust heterometallic ultramicroporous MOF with ultrahigh selectivity for propyne/propylene separation. *J Mater Chem A* 2021;9:2850-6. DOI
58. Gao J, Cai Y, Qian X, et al. A microporous hydrogen-bonded organic framework for the efficient capture and purification of propylene. *Angew Chem Int Ed Engl* 2021;60:20400-6. DOI
59. Zhou J, Ke T, Steinke F, et al. Tunable confined aliphatic pore environment in robust metal–organic frameworks for efficient separation of gases with a similar structure. *J Am Chem Soc* 2022;144:14322-9. DOI
60. Shi R, Lv D, Chen Y, et al. Highly selective adsorption separation of light hydrocarbons with a porphyrinic zirconium metal–organic framework PCN-224. *Sep Purif Technol* 2018;207:262-8. DOI
61. Huang Y, Lin Z, Fu H, et al. Porous anionic indium-organic framework with enhanced gas and vapor adsorption and separation ability. *ChemSusChem* 2014;7:2647-53. DOI
62. Zhang Y, Yang L, Wang L, Duttwyler S, Xing H. A microporous metal–organic framework supramolecularly assembled from a Cu^{II} dodecaborate cluster complex for selective gas separation. *Angew Chem Int Ed Engl* 2019;58:8145-50. DOI
63. Zhang Y, Yang L, Wang L, Cui X, Xing H. Pillar iodination in functional boron cage hybrid supramolecular frameworks for high performance separation of light hydrocarbons. *J Mater Chem A* 2019;7:27560-6. DOI
64. Li YZ, Wang GD, Krishna R, et al. A separation MOF with O/N active sites in nonpolar pore for one-step C_2H_4 purification from C_2H_6 or C_3H_6 mixtures. *Chem Eng J* 2023;466:143056. DOI
65. Xiao Y, Hong AN, Chen Y, et al. Developing water-stable pore-partitioned metal–organic frameworks with multi-level symmetry for high-performance sorption applications. *Small* 2023;19:2205119. DOI
66. Liu X, Hao C, Li J, et al. An anionic metal–organic framework: metathesis of zinc(II) with copper(II) for efficient C_3/C_2 hydrocarbon and organic dye separation. *Inorg Chem Front* 2018;5:2898-905. DOI
67. Zhang L, Ma L, Wang G, Hou L, Zhu Z, Wang Y. A new honeycomb MOF for C_2H_4 purification and C_3H_6 enrichment by separating methanol to olefin products. *J Mater Chem A* 2023;11:2343-8. DOI